Spectroscopic Study of H_2 and CO Adsorption on Platinum-Promoted Sulfated Zirconia Catalysts

Ping Wang,[†] Shuwu Yang,[†] Junko N. Kondo,[†] Kazunari Domen,*[,†] Takashi Yamada,[‡] and Hideshi Hattori[‡]

Chemical Resources Laboratory, Tokyo Institute of Technology, 4259 Nagatsuta, Midori-ku, Yokohama 226-8503, Japan, and Center for Advanced Research of Energy Technology, Hokkaido University, Sapporo 060-8628, Japan

Received: May 9, 2003; In Final Form: August 11, 2003

H_2 adsorption over two $Pt/SO_4^{2-}-ZrO_2$ (Pt/SZ) samples pretreated under different conditions (one is catalytically active and the other is inactive in *n*-butane isomerization) was investigated by in-situ Fourier transform infrared (FTIR) spectroscopy and temperature-programmed desorption (TPD). It was found that the formation of H_2O was the crucial difference between the active and inactive Pt/SZ samples upon H_2 adsorption at 523 K, with isolated zirconium OH groups forming on both samples. Under the same conditions, neither H_2O nor zirconium OH groups formed on $SO_4^{2-}-ZrO_2$ (SZ), and only a small amount of OH groups formed on Pt/ZrO_2. CO adsorption results reveal the presence of both Brϕnsted and Lewis acid sites on the surface of Pt/SZ, as well as the transformation of Lewis acid sites to Brϕnsted acid sites upon H_2 adsorption at 523 K. These results present direct evidence of H_2 spillover from Pt to the sulfated zirconia surface. The formation mechanism of H_2O and OH groups is discussed, and it is suggested that the active oxygen species, which should be associated with the intermediate sulfate species on the active Pt/SZ surface, plays an essential role as active sites on Pt/SZ in *n*-butane isomerization.

1. Introduction

Ever since sulfate-treated zirconia gels with and without a platinum promoter were reported to be active for paraffin isomerization in 1962,[1] catalysts based on sulfated zirconia have drawn much attention. The strong acidity and exceptionally high activity of $SO_4^{2-}-ZrO_2$ (SZ) makes this material attractive as a potential process catalyst in several acid-catalyzed reactions such as hydroisomerization, hydrocracking, alkylation, and oligomerization under mild conditions. Recent reviews on this remarkable catalyst can be found in the literature.[2−7] SZ is similar to other solid-acid catalysts in that is suffers from fast deactivation, presumably due to coke formation. The addition of a small amount of platinum to SZ has been found to be effective in suppressing this coke formation and thus in maintaining high activity for a longer time in the presence of H_2.[8]

Although numerous studies have been conducted on the physical and chemical properties and applications of SZ and $Pt/SO_4^{2-}-ZrO_2$ (Pt/SZ), several issues remain unresolved, including the nature of the active sites, the acidity and acid strength, as well as the role of hydrogen. The acidity of SZ is a key issue, whether Brϕnsted acid sites or Lewis acid sites, or both, are responsible for the catalytic activity of SZ and metal-promoted SZ catalysts. The unique catalytic activity of SZ and Pt/SZ has long been considered to be due to superacidity. However, recent theoretical calculations and/or test reactions by several authors have indicated that SZ is a strong acid with an acid strength similar to H-ZSM-5 or pure H_2SO_4, but is not a superacid.[9−11] As the traditional techniques widely used to characterize the acid strength of conventional solid-acid catalysts such as oxides and zeolites are not suitable for the SZ system, a means for defining and assessing the acid strength of SZ catalysts is a topic worthy of investigation.

The role of hydrogen is another important topic. Usually, platinum supported by a solid acid (e.g., Pt/zeolite) behaves as a bifunctional catalyst.[12] Such catalysts exhibit a rate equation with a negative order in hydrogen for the skeletal isomerization of alkanes because the initial dehydrogenation step is unfavorable in the presence of H_2. However, this is not always the case for Pt/SZ. Some authors[13,14] found that the skeletal isomerization of *n*-pentane and *n*-heptane over Pt/SZ is in fact positivly affected by H_2 partial pressure. More recently, Satoh et al.[15] found that hydrogen uptake on Pt/SZ is very high above 473 K, far exceeding the H/Pt unity ratio. This phenomenon can be well explained by hydrogen spillover from Pt to the sulfated zirconia support. Hattori[16] proposed that H_2 adsorption on Pt/SZ can be divided into four steps: (1) dissociation of molecular H_2 on Pt to form H atoms; (2) spillover of H atoms from Pt to the support; (3) migration of spilt-over hydrogen on the support to Lewis acid sites; and (4) extraction of electrons from H atoms by Lewis acid sites to form acidic protons and hydrides. To date, no direct evidence has been obtained to support the formation of these species, and the existence of such a relationship between the acidity of Pt/SZ and its hydrogen uptake ability remains unanswered.

The degree of dehydration of SZ-based catalysts is also an important factor determining catalytic activity. A plot of activity versus the amount of water adsorbed on the catalyst under working conditions exhibits a volcano-shaped curve.[17] Song and Kydd[18] studied the effect of water content on activity in *n*-butane isomerization and found that a small amount of water promoted

* Corresponding author. Tel: +81-45-924 5238. Fax: +81-45-924 5282. E-mail: kdomen@res.titech.ac.jp.
[†] Tokyo Institute of Technology.
[‡] Hokkaido University.

10.1021/jp030607c CCC: $25.00
Published on Web 10/08/2003

catalytic activity, while excess water had a negative effect. Dumesic and co-workers,[19−21] Keogh et al.,[22] and Pines[23] came to the same conclusions on the effect of water in SZ systems. The present authors' previous work[13,24] showed that as-prepared Pt/SZ pretreated at 573 K exhibits high activity for *n*-butane isomerization, while catalysts pretreated at 673 K or above completely lost this activity.

The purpose of this work was to directly observe the hydrogen spillover phenomenon by Fourier transform infrared (FTIR) spectroscopy and to compare hydrogen adsorption over Pt/SZ with different degrees of dehydration (one is catalytically active and the other is inactive in *n*-butane isomerization), SZ as well as Pt/ZrO_2, in order to correlate hydrogen uptake ability with acidity and elucidate the nature of active sites on this well-known catalyst.

2. Experimental Section

2.1. Catalyst Preparation. Catalysts were prepared as follows. $SO_4^{2-}-Zr(OH)_4$ was prepared by impregnation of 6 g of $ZrO_2 \cdot nH_2O$ with 10 mL of 1 N H_2SO_4 aqueous solution followed by filtration and drying at 383 K for 24 h. The sulfated zirconia ($SO_4^{2-}-ZrO_2$) was obtained by calcinating the $SO_4^{2-}-Zr(OH)_4$ at 873 K in air for 3 h.

Platinum was supported on the prepared $SO_4^{2-}-ZrO_2$ by impregnation of the calcined $SO_4^{2-}-ZrO_2$ with H_2PtCl_6 aqueous solution followed by drying at 383 K for 24 h and calcination at 873 K in air for 3 h. The BET surface area of the as-prepared Pt/SZ was 118 m^2/g, with 0.5% Pt and 1.9% S by elemental analysis.

Sulfate-free Pt/ZrO_2 was prepared by impregnation of ZrO_2 obtained by calcination of $ZrO_2 \cdot nH_2O$ at 873 K with H_2PtCl_6 aqueous solution followed by drying at 383 K and calcination at 723 K in air. The Pt content was adjusted to 0.5%.

2.2. Infrared Investigations. Each catalyst was pressed into a self-supporting wafer (ca. 20 mg/cm^2) and placed in the center of a quartz IR cell equipped with NaCl windows and connected to a conventional glass vacuum system capable of a final vacuum of $\sim 1 \times 10^{-5}$ Torr. The catalyst was prereduced with H_2 at 573 K for 2 h, followed by evacuation at either 573 or 723 K for 2 h, labeled Pt/SZ300 and Pt/SZ450, respectively. As Pt/SZ300 exhibited high activity for *n*-butane isomerization, whereas Pt/SZ450 had no activity, these are also referred to as the active catalyst and inactive catalyst, respectively.

For H_2 adsorption, H_2 (100 Torr) was introduced into the IR cell at desired temperatures after purification by passage through a liquid-nitrogen trap for at least 30 min. CO was purified using this liquid-nitrogen trap through several freeze−pump−thaw cycles. All IR spectra were recorded on a JASCO WS/IR-7300 spectrometer with a mercury cadmium telluride (MCT) detector. A total of 64 scans were collected at 4 cm^{-1} resolution for each spectrum. Unless otherwise indicated, the IR spectra given here are differential spectra obtained by subtracting the background spectra taken before H_2 or CO adsorption. In the following, "hydrogen-adsorbed" refers to Pt/SZ300 or Pt/SZ450 after H_2 adsorption at 523 K for 2 h followed by evacuation of gaseous H_2 at room temperature.

2.3. X-ray Diffraction Measurements. X-ray diffraction (XRD) patterns were obtained using a Rigaku RINT 2100 diffractometer with Ni filtration and Cu Kα radiation. No special protection was applied after pretreatment for the prereduced samples.

2.4. Temperature-Programmed Desorption (TPD) Measurements. After hydrogen adsorption on Pt/SZ300 or Pt/SZ450 at 523 K for 2 h, the samples were cooled to room temperature and then evacuated to pump off gaseous H_2 for 1 h. Temperature-programmed desorption (TPD) experiments were carried out from room temperature to 773 K under evacuation at a heating rate of 5 K/min. For comparison, TPD measurements were also performed on blank Pt/SZ300 and Pt/SZ450 under identical conditions.

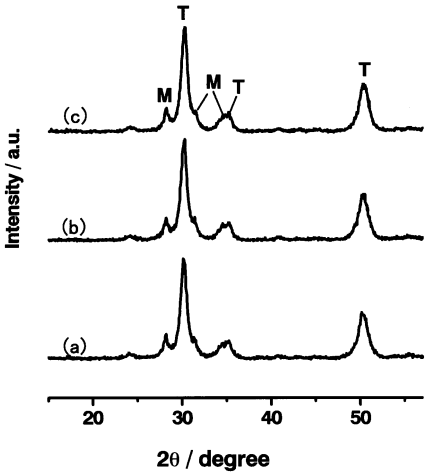

Figure 1. XRD patterns of (a) as-prepared Pt/SZ, (b) Pt/SZ300, and (c) Pt/SZ450.

3. Results and Discussion

3.1. XRD Results. The crystalline structure of SZ is one of the key factors affecting the catalytic activity of Pt/SZ. Most catalytically active SZ or Pt/SZ samples are predominantly composed of tetragonal-phase ZrO_2, whereas monoclinic samples have typically very low or no activity for *n*-butane isomerization.[25,26] Preparation conditions such as precursors, sulfur content, preparation method, as well as calcination temperature, can influence the final crystalline structure of Pt/SZ. The XRD patterns shown in Figure 1 reveal that the as-prepared Pt/SZ is primarily tetragonal, with a trace monoclinic phase. Pt particles were too small to be detected. Both Pt/SZ300 and Pt/SZ450 have a crystalline structure similar to that of the original Pt/SZ, demonstrating that the present activation (evacuation) temperature does not alter the crystalline phase. Also, the crystalline structure of Pt/SZ was confirmed by XRD to remain unchanged after being pressed into an IR disk in the present work. Therefore, differences due to crystallinity can be excluded as an explanation of the different activities of Pt/SZ300 and Pt/SZ450.

Elemental analysis revealed that both Pt/SZ300 and Pt/SZ450 have similar S contents, 1.5% and 1.4%, respectively, which is a little lower than that before pretreatment. Differences in activity for these two specimens must therefore be associated with other factors, such as the degree of dehydration, rather than crystallographic or elemental differences.

3.2. Background IR spectra of Pt/SZ. The as-prepared Pt/SZ samples were cooled and stored in air under ambient conditions without special protection after calcination at high temperature. Thus, it is inevitable that the samples will have adsorbed moisture from the atmosphere. Figure 2A shows the as-observed background IR spectra for Pt/SZ samples evacuated at different temperatures. All spectra were collected at 523 K. The spectra are very similar to those of non-platinum-loaded SZ (not shown).

The spectrum Figure 2A(a) represents the sample evacuated from room temperature to 523 K only. In the high-frequency region (4000−2500 cm^{-1}), a very strong broad band at ca.

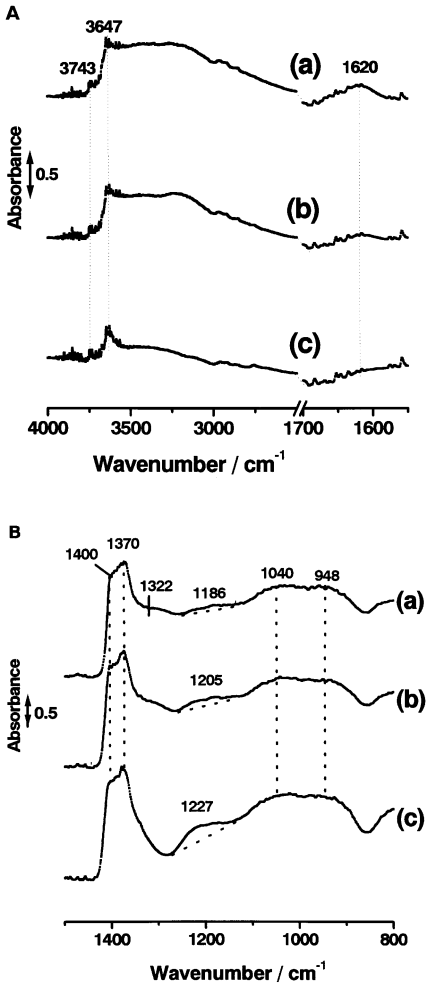

Figure 2. IR background spectra of (a) Pt/SZ heated from room temperature to 523 K under evacuation, (b) Pt/SZ300, and (c) Pt/SZ450. (A) OH stretching region, (B) sulfate region.

3600−2800 cm^{-1} is attributed to the presence of hydrogen-bonded OH groups and strongly bound water molecules, as evidenced by the appearance of the bending mode of H_2O at 1620 cm^{-1}. Two additional bands, a weak peak at 3743 cm^{-1} and a strong peak at 3647 cm^{-1}, can also be identified and assigned to the terminal and bridging zirconium OH groups, respectively. The intensity difference is indicative of the prevalence of the tetragonal phase;[27] the intensity of the terminal OH band is quite strong for the pure monoclinic phase. Compared with the spectrum for pure ZrO_2,[28] in which zirconium OH groups appear at 3774 and 3672 cm^{-1}, the isolated OH bands observed here are shifted to lower frequencies. This shift has been attributed to surface inductive effects induced by the presence of charge-withdrawing sulfates on Pt/SZ.[27]

For the catalytically active sample, Pt/SZ300 (Figure 2A(b)), elimination of the strongly bound water molecules and a fraction of the surface OH species at the higher evacuation temperature results in an almost complete disappearance of the band at 1620 cm^{-1} and a significant weakening of the broad band at ca. 3600−2800 cm^{-1}. For the catalytically inactive sample, Pt/SZ450 (Figure 2A(c)), the broad band at around 3600−2800 cm^{-1} is almost unrecognizable, and only the isolated terminal and bridging zirconium OH groups are detected.

In the sulfate region (1500−800 cm^{-1}, Figure 2B), the spectra for all Pt/SZ samples are similar and quite complex. Many researchers have assigned the band at about 1400−1360 cm^{-1} to the asymmetric stretching of S═O, and the band at 1050−900 cm^{-1} to the S−O asymmetric stretching vibration, due primarily to resolution limitations. However, the spectral change in this region depends greatly on the evacuation temperature and reflects the conversion of sulfur species. In Figure 2B(a), four bands at 1400, 1370, 1040 and 948 cm^{-1} are observed. Two additional bands at about 1322 and 1186 cm^{-1}, which occur as shoulders of the bands at 1370 and 1040 cm^{-1}, can also be identified. With increasing evacuation temperature, the intensity or band position of these four bands in Figure 2B((b) and (c)) remains unchanged. It is worthy noting that the two shoulder bands are strongly modified in a small range of evacuation temperature. The band at 1322 cm^{-1} strengthens slightly for Pt/SZ300 (Figure 2B(c)), but is almost completely nonexistent for Pt/SZ450 (Figure 2B(c)). The band at 1186 cm^{-1} in Figure 2B(a) strengthens and progressively shifts to higher frequencies, appearing at 1205 cm^{-1} in Figure 2B(b) and 1227 cm^{-1} in Figure 2B(c).

A few authors have mentioned the appearance of "transition" sulfate species during the heating of SZ from room temperature to 723 K under evacuation. Babou et al.[29] reported similar results and assigned these bands to different sulfur species. By studying the acidic properties of SZ through IR spectroscopy and theoretical calculation using ab initio methods, Babou et al. emphasized that the SZ catalyst could be described as an H_2SO_4 compound grafted onto the surface of zirconia in such a way that renders the catalyst highly sensitive to water in a reversible way. In intermediate dehydration conditions, three sulfur species—$(H_2SO_4)_{ads}$, $(HSO_4^-)_{ads}$, and $(SO_3)_{ads}$—coexist on the surface of the zirconia support. Accordingly, the presently observed bands at 1400 and 948 cm^{-1} can be expected to be due to the asymmetric S═O and S−O stretching vibrations of $(SO_3)_{ads}$, the bands at 1370 and 1040 cm^{-1} can be attributed to the asymmetric S═O and S−O stretching vibrations of $(H_2SO_4)_{ads}$, and the shoulder band at 1322 cm^{-1} will be due to the intermediate $(HSO_4^-)_{ads}$ species.

The S−OH bending vibration expected near 1180 cm^{-1} on SZ was not directly observed by Babou et al.[29] due to the strong hydrogen bonding to the surface and poorly resolved spectra in the sulfated stretching region, a problem also encountered by a number of other researchers.[30−32] From the present results, another reason may be the limited occurrence of S−OH groups in a very narrow temperature range. In this case, the two shoulder bands at 1322 and 1186−1205 cm^{-1} in the background spectra of Pt/SZ300 in Figure 2B, (a) and (b), can be assigned to the intermediate $(HSO_4^-)_{ads}$ species, which can only be present on the Pt/SZ surface within a narrow range of evacuation temperature and may play an important role as active sites on Pt/SZ, as will be discussed later. Chen et al.[33] also claimed the existence of $(HSO_4^-)_{ads}$ by adsorption of H_2O and NH_3 on SZ.

On the basis of the above discussion, the assignments of the observed IR bands on Pt/SZ activated at different temperatures are summarized in Table 1. The terminal bridging zirconia OH groups, and sulfate species $(H_2SO_4)_{ads}$ and $(SO_3)_{ads}$ were present on the surface of both active Pt/SZ300 and inactive Pt/SZ450 catalysts, while the intermediate sulfate species $(HSO_4^-)_{ads}$ and broad band at around 3600−2800 cm^{-1} due to hydrogen-bonded OH groups were observed only on the active Pt/SZ300 surface.

3.3. H_2 Adsorption. Figures 3 and 4 show the IR spectra for Pt/SZ300 and Pt/SZ450 after H_2 adsorption at 523 K. The progressive formation of zirconium OH groups, characterized by the appearance of two IR bands at 3740 and 3652 cm^{-1} due to the stretching vibrations of terminal and bridging zirconium OH groups, respectively, can be clearly observed with increasing

TABLE 1: Assignments of As-Observed IR Bands on Pt/SZ Activated at Different Temperatures[a]

IR bands (cm^{-1})	assignment	species	Pt/SZ250[b]	Pt/SZ300	Pt/SZ450
3743, *w*	ν_{OH}	terminal Zr−OH	+	+	+
3647, *s*	ν_{OH}	bridging ZrOH	+	+	+
2800−3600, *br*	ν_{OH}	H-bonded OH and H_2O	+	+	−
1620, rw	δ_{HOH}	H-bonded H_2O	+	tr	−
1400, *s*	$\nu^{as}_{S=O}$	$(SO_3)_{ads}$	+	+	+
1370, *s*	$\nu^{as}_{S=O}$	$(H_2SO_4)_{ads}$	+	+	+
1322, *sh*	$\nu^{as}_{S=O}$	$(HSO_4)_{ads}$	+	+	−
1227, *w*	$\nu^{s}_{S=O}$	$(H_2SO_4)_{ads}$	−	−	+
1205, *sh*	δ_{S-OH}	$(HSO_4)_{ads}$	−	+	−
1186, *sh*	δ_{S-OH}	$(HSO_4)_{ads}$	+	−	−
1040, *s*	ν^{as}_{S-O}	$(H_2SO_4)_{ads}$	+	+	+
948, *s*	ν^{as}_{S-O}	$(SO_3)_{ads}$	+	+	+

[a] *w*: weak, *s*: strong, *rw*: rather weak, *sh*: shoulder, *tr*: trace, +: presence, −: absence. [b] Refers to the Pt/SZ catalyst activated from room temperature to 523 K under vacuum.

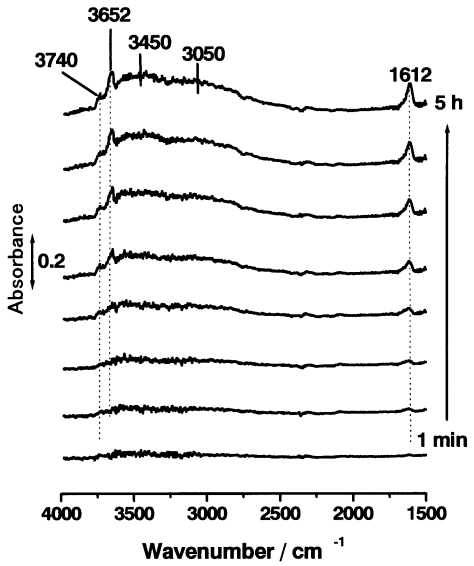

Figure 3. Adsorption of H_2 (100 Torr) on Pt/SZ300 at 523 K.

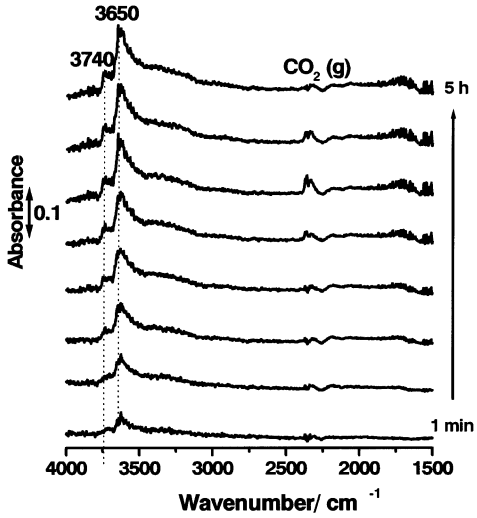

Figure 4. Adsorption of H_2 (100 Torr) on Pt/SZ450 at 523 K.

adsorption time. On Pt/SZ300 (Figure 3), two additional broad bands at ca. 3450 and 3050 cm^{-1} were also detected, along with a band at 1612 cm^{-1}. For the inactive sample, Pt/SZ450 (Figure 4), the spectra only revealed the occurrence of isolated terminal and bridging zirconium OH groups with IR bands at 3740 and 3650 cm^{-1} under the same conditions of H_2 adsorption. Therefore, the presence or absence of the species with IR bands

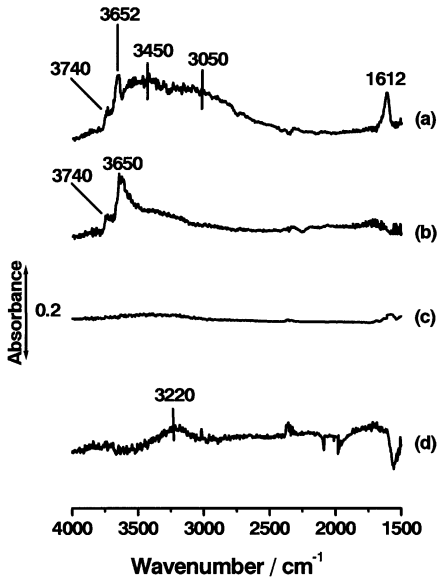

Figure 5. Adsorption of H_2 (100 Torr) on (a) Pt/SZ300, (b) Pt/SZ450, (c) SZ, and (d) Pt/ZrO_2 at 523 K for 2 h.

at 3450 (broad), 3050 (broad), and 1612 cm^{-1} upon H_2 adsorption is a crucial difference between active and inactive Pt/SZ catalysts.

Hydrogen adsorption on the non-Pt-loaded sample (SZ) and sulfate-anion-free sample (Pt/ZrO_2) was performed for comparison, and the results are summarized in Figure 5 (spectra (c) and (d)). The spectrum of SZ remained almost unchanged after adsorption of H_2. For Pt/ZrO_2, only a very weak band appeared centered around 3220 cm^{-1} due to the formation of hydrogen-bonded zirconium OH groups. The present results coincide well with the H_2 uptake profiles.[15] Without the presence of SO_4^{2-}, the rate of hydrogen uptake at 523 K on Pt/ZrO_2 was small compared to that on SO_4^{2-}-promoted Pt/ZrO_2. Without Pt, hydrogen uptake on SZ was negligible. It appears that the presence of SO_4^{2-} contributes to the hydrogen uptake rate, and that the presence of Pt is essential for hydrogen uptake.

TPD measurements were carried out to study the desorption behavior of the species formed upon H_2 adsorption. Figure 6 shows the hydrogen ($m/e = 2$) and H_2O ($m/e = 18$) desorption profiles from hydrogen-adsorbed Pt/SZ300 (after subtraction of blank Pt/SZ300) and from hydrogen-adsorbed Pt/SZ450 (after subtraction of blank Pt/SZ450). Although the H_2 desorption peaks appear at the same temperature (493 K) for the two samples, the H_2 peak from hydrogen-adsorbed Pt/SZ300 is appreciably weaker than that from hydrogen-adsorbed Pt/SZ450.

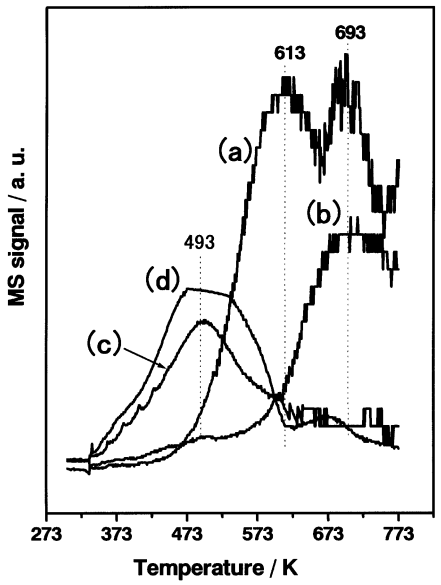

Figure 6. TPD profiles of hydrogen-adsorbed Pt/SZ. (a) H_2O from hydrogen-adsorbed Pt/SZ300, (b) H_2O from hydrogen-adsorbed Pt/SZ450, (c) H_2 from hydrogen-adsorbed Pt/SZ300, and (d) H_2 from hydrogen-adsorbed Pt/SZ450.

The desorption peaks for H_2O clearly differ for the two samples. A considerable amount of H_2O desorbed from Pt/SZ300 below 573 K (pretreatment temperature), which is considered to be responsible for the subsequent IR bands at 3450, 3050, and 1612 cm^{-1}. On the other hand, only a small amount of H_2O desorbed from Pt/SZ450 below 723 K (pretreatment temperature), attributed to the production of H_2O from isolated OH groups.

An H/D isotopic exchange experiment was carried out for the hydrogen-adsorbed Pt/SZ300 sample in order to elucidate the assignments of the three IR bands at 3450, 3050, and 1612 cm^{-1}. D_2 (400 Torr) was introduced at 373 K into the IR cell holding the hydrogen-adsorbed Pt/SZ300 (spectrum shown in Figure 5(a)). Figures 7A and 7B show the spectral changes during the isotopic exchange reaction. The terminal and bridging OH groups were gradually converted into their OD forms, which appear as peaks at 2768 and 2694 cm^{-1}. The three bands at 1612, 3050, and 3450 cm^{-1} weakened, and three new complementary bands gradually appeared at ca. 1418, 2400, and 2512 cm^{-1}. The vibrational frequency ratios of the latter two bands before and after isotopic exchange are 1.270 and 1.373, respectively, while that of the first band is 1.137 (1612/1418). This isotopic effect is the same as that of water,[34] which suggests that the three bands may be due to the formation of H_2O: bands at 2400 and 2512 cm^{-1} correspond to OD stretching, and the band at 1418 cm^{-1} represents the HDO bending mode. No band attributable to δ_{D2O} was identified because of the poor resolution of the spectra at ca. 1190 cm^{-1}.

The wide tailing of the OH stretching band of the presently observed H_2O to low frequency ($\sim$2800 cm^{-1}) is distinguished from generally observed water adsorbed on oxides. This may be due to the presence of strong hydrogen-bonding interaction with the SZ surface and also formation of water clusters. Morterra et al.[35] expounded the possibility in assigning the similar bands on SZ to $[H_3O]^+$ species. However, up to now no unambiguous IR spectral identification of $[H_3O]^+$ species on the surface of a catalytic system such as SZ is available. Here, we tentatively attribute the three bands at 3450, 3050, and 1612 cm^{-1} to H_2O.

The formation of H_2O on Pt/SZ300 upon H_2 adsorption resulted in the elimination of oxygen atoms during H_2 adsorption and successive desorption. As a result, the rate of formation of H_2O on Pt/SZ300 due to H_2 adsorption decreased with repetition of the adsorption−desorption cycles, as shown later. A comparison of the TPD results and the IR spectra for H_2 adsorption on Pt/SZ300 (Figure 5(a)) and Pt/SZ450 (Figure 5(b)) clearly revealed that H_2O forms on the former but not on the latter, indicating that the active surface oxygen species responsible for the formation of H_2O upon interaction with H_2 are liberated as H_2O during evacuation at 723 K to form the inactive Pt/SZ450.

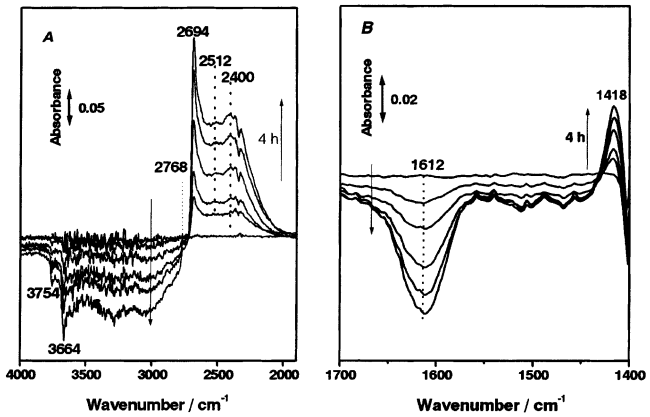

Figure 7. H/D isotopic exchange on hydrogen-adsorbed Pt/SZ300 (spectrum shown in Figure 5a) at 373 K. (A) OH/OD stretching region, (B) HOH bending region.

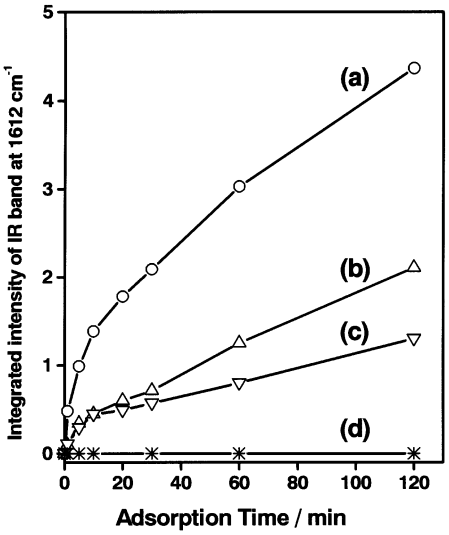

Figure 8. Integrated intensity of 1612 cm^{-1} band versus H_2 adsorption time (100 Torr) with increasing adsorption−desorption repetition cycles for Pt/SZ300 at 573 K: (a) run 1, (b) run 2, (c) run 3, and (d) subsequent evacuation at 723 K followed by H_2 adsorption at 573 K for 2 h. Hydrogen-adsorbed Pt/SZ300 was evacuated at 573 K for 2 h at each interval.

3.4. Reproducibility of the Formation of H_2O on Pt/SZ300. The reproducibility of the formation of H_2O on Pt/SZ300 was investigated as follows. H_2 was adsorbed on Pt-SZ300 at 573 K for 2 h, followed by evacuation for 2 h at the same temperature. This process was repeated three times (runs 1 to 3). The variation in integrated intensity of the band at 1612 cm^{-1} over the three cycles is shown in Figure 8. As already shown in Figure 3, for hydrogen adsorption on Pt/SZ300, the gradual formation of zirconium OH bands and the bands assigned to H_2O were observed in all three runs. The integrated intensity of the band at 1612 cm^{-1} decreased successively in each run (run 1 > run 2 > run 3).

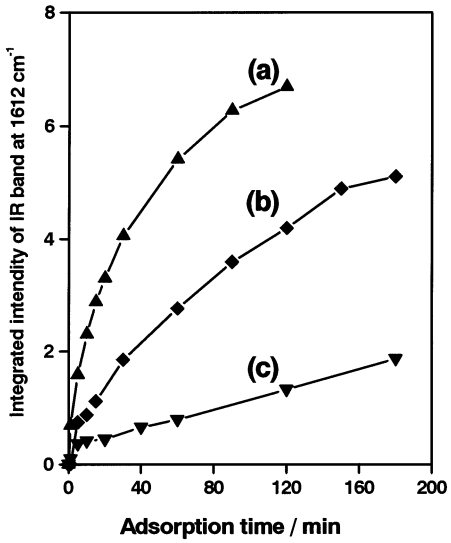

Figure 9. Variation in integrated intensity of d_{H_2O} (1612 cm^{-1}) band with H_2 adsorption (400 Torr) time for Pt/SZ300 at (a) 573 K, (b) 553 K, and (c) 523 K.

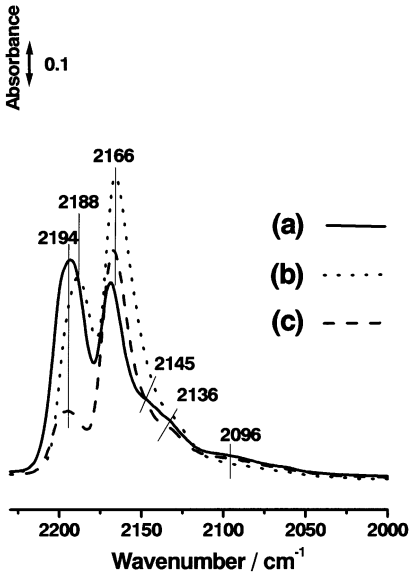

Figure 10. CO adsorption at 150 K on Pt/SZ300 (a) before and (b) after hydrogen adsorption at 523 K (CO adsorption was carried out after elimination of gaseous H_2 at room temperature), and (c) H_2O-covered Pt/SZ300.

After the third run, the sample was evacuated at 723 K and then exposed to hydrogen at 573 K for 2 h. In this case, results similar to those observed upon H_2 adsorption on Pt/SZ450 (Figure 4) were obtained. No bands due to H_2O (Figure 8(d)) were detected, only those attributable to terminal and bridging zirconium OH groups. This confirms that the surface-active oxygen responsible for the formation of H_2O on Pt/SZ300 upon interaction with H_2 becomes less and less abundant with repetition of H_2 adsorption and successive desorption, and that the active oxygen species are removed by evacuation at 723 K to form the inactive Pt/SZ. However, when the inactive Pt/SZ450 sample was loaded with a suitable amount of water followed by H_2 adsorption, as in the case of the fresh Pt/SZ300, spectra similar to those in Figure 3 are observed, although with lower intensity of the three bands at 3450, 3050, and 1612 cm^{-1} (the intensity of the band at 1612 cm^{-1} is about 30% of that in Figure 8(a) after H_2 adsorption for 120 min). Therefore, the loading of a trace amount of water can partially restore the inactive Pt/SZ450 to its active form Pt/SZ300, demonstrating the reversibility of the effect of water on the generation of surface-active oxygen species responsible for the formation of H_2O upon H_2 adsorption.

H_2 adsorption on Pt/SZ300 was performed at different temperatures between 493 and 573 K to estimate the energy barrier for the formation of OH groups and water. The integrated intensity of the 1612 cm^{-1} band at different temperatures is shown with respect to reaction time in Figure 9. Higher temperature is beneficial for the formation of the species indicated by the IR band at 1612 cm^{-1}, and the activation energy is roughly estimated to be 183 $\pm$ 10 kJ/mol in the range 493−573 K according to the Arrhenius equation. The authors have previously reported in the kinetic analysis of hydrogen adsorption on Pt/SZ300 that the slow step in hydrogen adsorption represents surface migration of spilt-over hydrogen, with an activation energy of 84 kJ/mol.[15] As the present activation energy is clearly higher, it is suggested that the H_2O formation step is slower than the migration step. The formation of H_2O should be in a way which will not affect the degree of hydrogen adsorption, effectively preventing this H_2O formation step from being detected by kinetic analysis.

3.5. CO Adsorption. CO is one of the most frequently used probe molecules in the study of Lewis acid sites and Brϕnsted acid sites on catalyst surfaces. Figure 10 shows the spectra for CO adsorption on Pt/SZ300 at 150 K before and after H_2 adsorption. When CO was adsorbed on Pt/SZ300 before H_2 adsorption (Figure 10(a)), five bands were identified at 2194, 2166, 2145, 2136, and 2096 cm^{-1} in the CO stretching region. The two weak bands at 2145 and 2136 cm^{-1} have been attributed to physically absorbed CO,[36] and the band at 2096 cm^{-1} has been ascribed to linearly adsorbed CO at Pt sites.[37] The bands at 2194 and 2166 cm^{-1} coincide with the positions of σ-coordinated CO on the surface unsaturated Zr^{4+} sites (Lewis acid sites) and CO hydrogen-bonded to OH groups (Brϕnsted acid sites), as evidenced by the shift of isolated bridging zirconium OH groups to hydrogen-bonded groups at about 3500 cm^{-1} (broad band, see Figure 11A).[36] CO adsorption also results in a negative band at ca. 3663 cm^{-1}.

As described in the Introduction, SZ possesses an acid strength similar to H-ZSM-5. As a preliminary investigation of the acidity of Pt/SZ, the shift of the OH bands ($\Delta\nu_{OH}$) after CO adsorption on Pt/SZ is compared with that for strong Brϕnsted-acidic H-ZSM-5 and Al_2O_3 in Table 2. The shift $\Delta\nu_{OH}$ after CO adsorption on Pt/SZ is larger than that on Al_2O_3 but smaller than that on H-SZM-5. However, this does not mean that the acidity of Pt/SZ is weaker than that of HZSM-5. Basic probe molecules such as CO are initially adsorbed at the Lewis acid sites of Pt/SZ, which weakens the Brϕnsted acidity of the bridging OH groups prior to interaction with CO. As a result, the observed $\Delta\nu_{OH}$ is unable to reveal the intrinsic acidity of Pt/SZ.

Figure 10(b) shows the IR spectrum for CO adsorption on hydrogen-adsorbed Pt/SZ300 at 150 K. The band at 2194 cm^{-1} in Figure 10(a) due to CO adsorbed at Lewis acid sites is weaker and shifts to 2188 cm^{-1}, while the intensity of the band at 2166 cm^{-1} due to CO hydrogen-bonded to OH groups is much higher. The integrated relative intensity ratio of the CO adsorbed at Brϕnsted acid sites to that at Lewis acid sites increased from 0.44 (Figure 10(a)) to 1.76 (Figure 10(b)), which strongly supports the formation of Brϕnsted acid sites and consumption of Lewis acid sites due to hydrogen adsorption on Pt/SZ300. When Pt/SZ300 was loaded with a trace amount of H_2O at room temperature and then exposed to CO (Figure 10(c)), the band at 2194 cm^{-1} weakened but did not shift. This clearly reflects

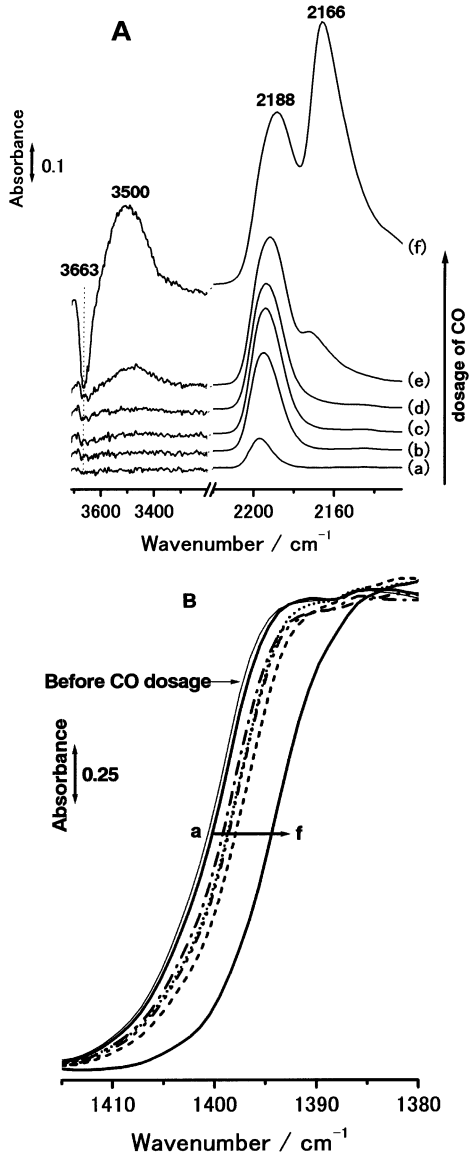

Figure 11. CO dosage on Pt/SZ300 at 150 K. (A) OH and CO stretching region (after background subtraction). (B) SO stretching region for (a) 0.13 mmol, (b) 0.76 mmol, (c) 1.13 mmol, (d) after CO saturated adsorption (10 Torr) followed by evacuation for 10 min at the same temperature (overlap with (c) in SO stretching region), (e) 2.12 mmol, and (f) CO saturated adsorption (10 Torr).

TABLE 2: Comparison of ν_{OH} and $\Delta\nu_{OH}$ after CO Adsorption on Pt/SZ and Other Solid Samples

sample	ν_{OH} (cm^{-1})	$\Delta\nu_{OH}$ (cm^{-1})	ref
Pt/SZ300	3644	−173	this work
Pt/SZ450	3642	−173	this work
SZ	3644	−144	this work
Pt/ZrO_2	not observed		this work
H-ZSM-5	3621	−304	38
γ-Al_2O_3	3695	−95	39

the difference between the surface of the hydrogen-adsorbed Pt/SZ300 and the H_2O-covered Pt/SZ300: upon H_2 adsorption, the spilt-over H atoms donate electrons to Lewis acid sites at 523 K, thereby weakening the charge density of Zr^{4+}, as discussed below.

In the sulfate region, CO adsorption results in the downward shift of the $\nu_{S=O}$ band at 1400 cm^{-1} (Figure 11B). Even dosing with trace amounts of CO, in which case CO only adsorbs at Lewis acid sites as shown in spectra (a)−(c) in Figure 11A, results in a shift of the band at 1400 cm^{-1} to lower frequency, implying that sulfate groups may be adjacent to Lewis acid sites. The sulfate groups are also closely associated with the Brønsted acid sites. As the dosage of CO is increased, a band at 2166 cm^{-1} due to hydrogen-bonded CO gradually appears, accompanied by the conversion of isolated OH groups to hydrogen-bonded OH (Figure 11A, (e) and (f)) and the continuous shift of the $\nu_{S=O}$ band. After liberation of hydrogen-bonded CO by evacuation, as evidenced by the absence of the negative band at 3663 cm^{-1}, the position of the $\nu_{S=O}$ band shifts upward but is not completely restored due to CO adsorbed irreversibly at Lewis acid sites at 150 K (Figure 11B(d)).

Although the hydride species (Zr−H, which has been observed in the previous work of our groups by H_2, CO, and CO_2 adsorption on ZrO_2[28,40]) expected to form due to H_2 spillover on Pt/SZ was not detected directly, the downward shift of the band at 2194 cm^{-1} (due to CO adsorbed on Zr^{4+}) to 2188 cm^{-1} after H_2 adsorption (Figure 10a,b) might suggest the formation of $Zr^{\delta+}$ ($0 < \delta < 4$) sites or Zr−H species. Generally, when CO is adsorbed on the surface of d^0 oxide systems at low temperature, one or more bands appear at 2250−2150 cm^{-1} in the IR spectrum. The shift (compared with free gas CO at 2143 cm^{-1}) depends on the strength of the bond formed between the carbon atom of CO and the charge-withdrawing surface center.[41] The shift of the CO stretching vibration from 2194 to 2188 cm^{-1} after hydrogen adsorption on Pt/SZ indicates that the CO−Zr^{4+} bond was weakened due to electron donation from H atoms to Zr^{4+} sites.

3.6. Acidity of Pt/SZ, SZ, and Pt/ZrO_2. As described in the Introduction, H_2 adsorption on Pt/SZ can be divided into four steps: (1) dissociation of molecular H_2 on Pt to form H atoms; (2) spillover of H atoms from Pt to the support; (3) migration of spilt-over hydrogen on the support to Lewis acid sites; and (4) extraction of electrons from H atoms by Lewis acid sites to form acidic protons and hydrides. In the present IR results, H_2O and/or OH groups were observed clearly on the Pt/SZ catalyst upon H_2 adsorption, representing direct evidence of the spillover of hydrogen from Pt to the support. The last step, extraction of electrons from H atoms by Lewis acid sites to form OH groups and H_2O, is considered to be critical. Hydrogen dissociation on Pt (step 1) is known to proceed readily, even at room temperature.[15] For SZ, neither OH groups nor H_2O were produced under the same conditions. This is reasonable because the Pt sites responsible for the dissociation of H_2 are absent. Both spillover of H atoms from Pt to the support (step 2) and migration of spilt-over hydrogen on the support to Lewis acid sites (step 3) should give rise to similar hydrogen adsorption ability for Pt/ZrO_2.

The hydrogen adsorption ability of Pt/ZrO_2 differs significantly from that of Pt/SZ. This difference is due to the presence of sulfate groups in the latter. Clearly, sulfate groups modify the surface properties of Pt/SZ, resulting in a high ability for generating OH groups and H_2O from spilt-over hydrogen atoms. The formation of Brønsted acid sites is associated with the reaction of Lewis acid sites with spilt-over hydrogen atoms.[16] In this case, the formation of Brønsted acid sites is directly related to the state of Lewis acid sites. If the Lewis acidity of Pt/SZ is strong, the catalyst will have be able to readily extract electrons from hydrogen, promoting the formation of Brønsted acid sites. It can thus be concluded from the present H_2 adsorption results that Pt/SZ has stronger Lewis acidity than Pt/ZrO_2. From TPD profiles of pyridine adsorption, Ebitani et al.[13] came to the same conclusion that Lewis acidity on Pt/SZ is stronger than that on either Pt/ZrO_2 or SZ. The Lewis acid

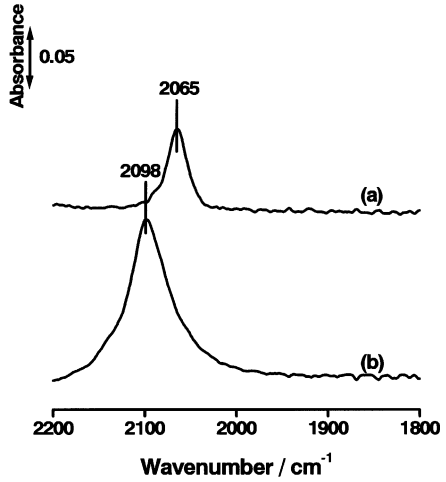

Figure 12. CO (CO 10 Torr) adsorption at room temperature on (a) Pt/ZrO_2 (after same pretreatment as Pt/SZ300 before CO adsorption), and (b) Pt/SZ300.

sites on SZ are also considered to be more acidic than those on un-promoted zirconia (pure ZrO_2).[31,42,43]

The sulfation of Pt/ZrO_2 also affects the electronic state of the Pt. In the room-temperature adsorption of CO on Pt/ZrO_2 pretreated under the same conditions as for Pt/SZ300, a band was observed at 2065 cm^{-1}, corresponding to the linearly adsorbed CO species at Pt sites as shown in Figure 12(a). A similar band appeared at 2098 cm^{-1} (Figure 12(b)) in the adsorption of CO on Pt/SZ300. This clearly demonstrates that the presence of sulfate species causes a change in the electron density of Pt on the SZ support.

3.7. Mechanism of Formation of H_2O and OH Groups on Pt/SZ. The formation of H_2O upon H_2 adsorption has been reported for Rh/Al_2O_3.[44] The H_2O formation mechanism in that case was postulated to be due to the combination of spilt-over H atoms with hydroxyl groups based on the concomitant weakening of the signal due to surface hydroxyl groups and growth of the band at 1612 cm^{-1} (δ_{H_2O}). The mechanism of the formation of H_2O and OH groups on Pt/SZ should differ from that of metal supported on oxides because the presence of sulfate groups modifies the surface of Pt/SZ significantly. As both Pt/SZ300 and Pt/SZ450 were reduced with H_2 at 573 K before H_2 adsorption, the water arising from the reduction of Pt oxides can be excluded. Therefore, the formation of H_2O is considered to be related to active oxygen, which is associated with the presence of intermediate sulfate species on the active Pt/SZ300.

When H_2 adsorbs onto the surface of Pt/SZ300, it first dissociates on Pt to form H atoms, followed by spillover to the zirconia support and migration to Lewis acid sites, where the H atoms lose electrons to form protons. These protons either combine with the neighboring (Zr)−O to form new OH groups, or react with the surface active oxygen associated with the intermediate sulfur species to form H_2O. When H_2 adsorbs onto the inactive Pt/SZ450 under the same conditions, the protons formed by the loss of electrons from spilt-over H atoms at Lewis acid sites can only combine with (Zr)−O to form OH groups, active oxygen species having been removed by evacuation at 723 K. Upon dosing the inactive sample with a suitable amount of H_2O, the population of active oxygen species will be partially restored. Thus, these active oxygen species associated with the intermediate sulfur species are considered to play an important role in *n*-butane isomerization on Pt/SZ in the presence of H_2.

4. Conclusions

The formation of terminal (3740 cm^{-1}) and bridging zirconium OH groups (3652 cm^{-1}) as well as H_2O (evidenced by a band at 1612 cm^{-1} and two additional broad bands centered around 3450 and 3050 cm^{-1}) was directly observed by in-situ FTIR spectroscopy for hydrogen adsorption on an active Pt/SZ catalyst. On the inactive catalyst, only isolated terminal and bridging zirconium OH groups were observable. CO adsorption results revealed the presence of both Brønsted acid sites and Lewis acid sites on the surface of Pt/SZ, as well as the transformation of Lewis acid sites to Brønsted acid sites upon hydrogen adsorption at 523 K. Red-shift of the band at 2194 cm^{-1} due to CO adsorption to Zr^{4+} after H_2 adsorption reflects the possible presence of $Zr^{\delta+}$ ($0 < \delta < 4$) sites or hydrides. The present IR results provide direct evidence of hydrogen spillover from platinum to the sulfated zirconia surface. The appearance of active oxygen, which is expected to be related to the intermediate sulfur species on the active Pt/SZ surface, was suggested to be responsible for the formation of H_2O upon adsorption of H_2 and may play an essential role in the high activity of Pt/SZ in *n*-butane isomerization.

Acknowledgment. This work was performed as a research project of the Japan Petroleum Institute commissioned by the Petroleum Energy Center and subsidized by the Ministry of Economy, Trade and Industry, Japan.

References and Notes

(1) Holm, V. C. F.; Bailey, G. C. U.S. Patent 3,032,599, 1962.
(2) Arata, K. *Adv. Catal*. **1990**, *37*, 165.
(3) Tanabe, K.; Misono, M.; Ono, Y.; Hattori, H. *Stud. Surf. Sci. Catal*. **1989**, *51*, 199.
(4) Tanabe, K.; Hattori, H.; Yamaguchi, T. *Crit. Rev. Surf. Chem.* **1990**, *1*, 1.
(5) Davis, B. H.; Keogh, R. A.; Srinivasan, R. *Catal. Today* **1994**, *20*, 219.
(6) Corma, A. *Chem. Rev.* **1995**, *95*, 559.
(7) Song, X. M.; Sarayi, A. *Catal. Rev.—Sci. Eng.* **1996**, *38* (3), 329. (b) Hammache, S.; Goodwin, J. G. *J. Catal.* **2003**, *218* (2), 258. (c) Garcia, E.; Volpe, M. A.; Ferreira, M. L.; Rueda, E. *J. Mol. Catal.* A: *Chemica* **2003**, *201* (1−2), 263. (d) Akkari, R.; Ghorbel, A. *Stud. Surf. Sci. Catal.* **2002**, *143*, 803. (e) Pakhomov, N. A.; Ivanova, A. S.; Bedilo, A. F.; Moroz, E. M.; Voldin, A. M. *Stud. Surf. Sci. Catal*. **2002**, *143*, 353.
(8) Baba, S.; Shibata, Y.; Kawamura, T.; Takaoka, H.; Kimura, T.; Kousaka, K.; Minato, Y.; Yokoyama, N.; Lida, K.; Imai, T. *EP* 174836, **1986**.
(9) Babou, F.; Bigot, B.; Coudurier, G.; Sautet, P.; Védrine, J. C. *Stud. Surf. Sci. Catal.* **1989**, *44*, 99.
(10) Babou, F.; Bigot, B.; Coudurier, G.; Sautet, P. *J. Phys. Chem.* **1993**, *97*, 11501.
(11) Umansky, B.; Engelhardt, J.; Hall, W. K. *J. Catal.* **1991**, *127*, 128.
(12) Iglesia, E.; Barton, D. G.; Biscardi, J. A.; Gines, M. J. L.; Soled, S. L. *Catal. Today* **1997**, *38*, 339.
(13) Ebitani, K.; Konishi, J.; Hattori, H. *J. Catal.* **1991**, *130*, 257.
(14) Iglesia, E.; Soled, S. L.; Kramer, G. M. *J. Catal.* **1993**, *144*, 238.
(15) Satoh, N.; Hayashi, J.-i.; Hattori, H. *Appl. Catal. A: General* **2000**, *202*, 207.
(16) Hattori, H. *Stud. Surf. Sci. Catal*. **2001**, *138*, 3.
(17) Babou, F.; Bigot, B.; Coudurier, G.; Sautet, P.; Védrine, J. C. *Stud. Surf. Sci. Catal.* **1994**, *90*, 519.
(18) Song, S. X.; Kydd, R. A. *J. Chem. Soc., Faraday Trans*. **1998**, *94*, 1333.
(19) González, M. R.; Kobe, J. M.; Fogash, K. B.; Dumesic, J. A. *J. Catal.* **1996**, *160*, 290.
(20) Kobe, J. M.; González, M. R.; Fogash, K. B.; Dumesic, J. A. *J. Catal.* **1996**, *164*, 459.
(21) González, M. R.; Fogash, K. B.; Kobe, J. M.; Dumesic, J. A. *Catal. Today* **1997**, *33*, 303.
(22) Keogh, R. A.; Srinivasan, R.; Davis, B. H. *J. Catal*. **1995**, *151*, 292.
(23) Pines, H. *The Chemistry of Catalytic Hydrocarbon Conversion*; Academic Press: New York, 1981.
(24) Ebitani, K.; Tsuji, J.; Hattori, H.; Kita, H. *J. Catal.* **1992**, *138*, 750.

(25) Morterra, C.; Cerrato, G.; Pinna, F.; Signoretto, M. *J. Catal*. **1995**, *157*, 109.
(26) Corma, A.; Juan-Rajadell, M. I.; López-Nieto, J. M.; Martínes, A.; Martínes, C. *Appl. Catal. A: General* **1994**, *175*, 111.
(27) Morterra, C.; Cerrato, G.; Ardizzone, S.; Bianchi, C. L.; Signoretto, M.; Pinna, F. *Phys. Chem. Chem. Phys*. **2002**, *4*, 3136.
(28) Kondo, J.; Sakata, Y.; Domen, K.; Maruya, K.; Onish, T. *J. Chem. Soc., Faraday Trans.* **1990**, *86*, 397.
(29) Babou, F.; Coudurier, G.; Vedrine, J. C. *J. Catal*. **1995**, *152*, 341.
(30) Adeeva, V.; de Haan, J. W.; Jänchen, J.; Lei, G. D.; Schünemann, G.; Van de Ven, L. J. M.; Sachtler, W. M. H.; van Santen, R. A. *J. Catal*. **1995**, *151*, 364.
(31) Waqif, M.; Bachelier, J.; Saur, O.; Lavalley, J.-C. *J. Mol. Catal*. **1992**, *72*, 127.
(32) Kustov, L. M.; Kazansky, V. B.; Figueras, F.; Tichit, D. *J. Catal*. **1994**, *150*, 143.
(33) Chen, F. R.; Coudurier, G.; Joly, J.-F.; Védrine, J. C. *J. Catal*. **1993**, *143*, 616.
(34) Pinchas S.; Laulicht I. *Infrared Spectra of Labeled Compounds*; *Academic Press*: New York, 1971; p 43.
(35) Morterra, C.; Cerrato, G.; Pinna, F.; Signoretto, M. *J. Phys. Chem*. **1994**, *98*, 12373.
(36) Spielbauer, D.; Mekhemer, G. A. H.; Zaki, M. I.; Knözinger, H. *Catal. Lett*. **1996**, *40*, 71.
(37) Dulaurent, O.; Bianchi, D. *Appl. Catal. A: General* **2001**, *207*, 211.
(38) Wakabayashi, F.; Kondo, J. N.; Domen K.; Hirose, C. *J. Phys. Chem.* **1995**, *99*, 10573.
(39) Zaki, M. I.; Knözinger, H. *Mater. Chem. Phys.* **1987**, *17*, 201.
(40) Kondo, J.; Abe, H.; Sakata, Y.; Maruya, K.; Domen, K.; Onishi, T. *J. Chem. Soc., Faraday Trans.* **1988**, *84*, 511.
(41) Morterra, C.; Cerrato, G.; Pinna, F. *Spectrochim. Acta, Part A* **1999**, *55*, 95.
(42) Bensitel, M.; Saur, O.; Lavalley, J. C. *Mater. Chem. Phys.* **1987**, *17*, 29.
(43) Srinivasan, R.; Keogh, R. A.; Milburn, D. R.; Davis, B. H. *J. Catal*. **1995**, *153*, 123.
(44) Wey, J. P.; Neely, W. C.; Worley, S. D. *J. Phys. Chem.* **1991**, *95*, 8881.